Electronic Supplementary Information (ESI)

Experimental section

Materials: All chemicals were purchased and used without purification. Copper foam (CF, 99.8%) was bought from Suzhou Sinero Technology Co., Ltd. Sodium hydroxide (NaOH, 97.0%), potassium hydroxide (KOH, 95.0%), ammonium persulfate ($(NH4)_2S_2O_8$, 99.0%), deuterium oxide (D_2O, 99.9%), ethylamine ($C_2H_5NH_2$, 68.0%-72.0% in H_2O), diethylamine ($(C_2H_5)_2NH$, 99.0%), triethylamine ($(C_2H_5)_3N$, 99.0%) were procured from Shanghai Meryer. Dimethyl sulfoxide (DMSO, 99.9%）was procured from Shanghai Aladdin, Acetonitrile (C_2H_3N, 99.5%) were procured from Sinopharm. Chemical Reagent Co., Ltd.

Synthesis of $Cu(OH)_2$ NWs on the copper foam: In a typical synthesis process, 2 × 4 cm^2 of CF was washed successively with acetone, 1.0 M HCl solution, and deionized water to clean the surface. Next, the washed CF was soaked in 0.13 M $(NH_4)_2S_2O_8$ with 2.78 M NaOH for 30 min at room temperature. The sample was then washed with deionized water and dried in an oven at 60 °C for 1 h to obtain Cu $(OH)_2$ NWs/CF. The obtained $Cu(OH)_2$ NWs/CF was subjected to anneal in flowing argon at 550 °C for 3 h (marked as Cu_2O/CF). The preparation process of CuO/CF was similar to that of Cu_2O/CF, except that the heat treatment conditions were changed to 180 °C for 1 h. Next, the CuO/CF was annealed in a 5% H_2/Ar flow atmosphere at 350 °C for 3 h to obtain Cu/CF.

Characterization

The morphologies and microstructural information were examined using an America FEI Nano Sem 200 scanning electron microscopy (SEM) at an accelerating voltage of 10 kV, and transmission electron microscopy (TEM, JEM-2100F, JEOL) was observed at a voltage of 200 kV. X-ray powder diffraction (XRD) analysis was conducted using a Bruker D8-Advance Davinci diffractometer with Cu Kα radiation for the identification of crystal structure. The surface chemical composition was analyzed using X-ray photoelectron spectroscopy (XPS, K-Alpha, Thermo Fisher Scientific). O_V were detected by electron paramagnetic resonance spectroscopy (EPR, Bruker A300). The liquid products were analyzed by ^1H NMR spectroscopy (NMR, Wuhan Zhongke Oxford Spectrum, 400MHz).

Electrochemical measurements

The electrochemical performance of the prepared catalysts was evaluated using a CHI 660E electrochemical workstation. The reaction was carried out in a typical H-type electrolytic cell, with Nafion 117 membrane used as the separator to separate the cathode and anode. Inject 30 mL of 1.0 M KOH electrolyte containing 8 wt% acetonitrile into the cathode, and add an equal volume of 1.0 M KOH electrolyte to the anode. The geometric area of the working electrode: 1.0 cm × 1.0 cm (the part immersed in the electrolyte). The standard three-electrode system was used for electrochemical measurements, in which prepared catalysts was used as the working electrode, Ag/AgCl electrode and graphite rod were used as the reference and counter electrodes, respectively.

Product detection and analysis

The sample was subjected to chronoamperometric testing at different working potentials (-0.25, -0.30, -0.35, -0.40, -0.45 and -0.50 VRHE) for 1 h. The FE of the liquid products were calculated using the following equation:

$$FE = \frac{n_{product} \times e \times F}{Q} \times 100\%$$

where *n* is the amount of product ethylamine in moles, *e* is the number of electrons transferred, *F* is the Faraday constant (96485 C mol^{-1}), *Q* is the total charge passing through the working electrode (the integral of the total reaction current and the reaction time).

$$\text{Yield calculation formula: Yield} = \frac{n_{product}}{t}$$

where *t* represents the time of the electrocatalytic ARR process.

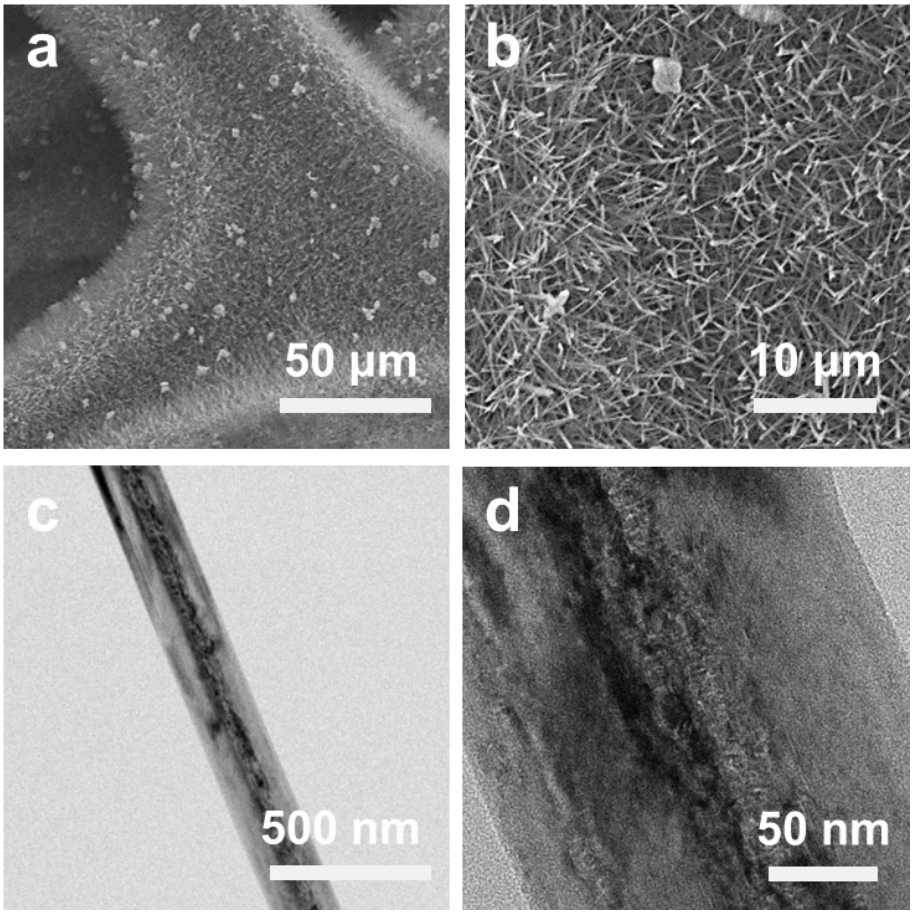

Fig. S1. (a, b) SEM images and (c, d) TEM images of $Cu(OH)_2$ NWs/CF.

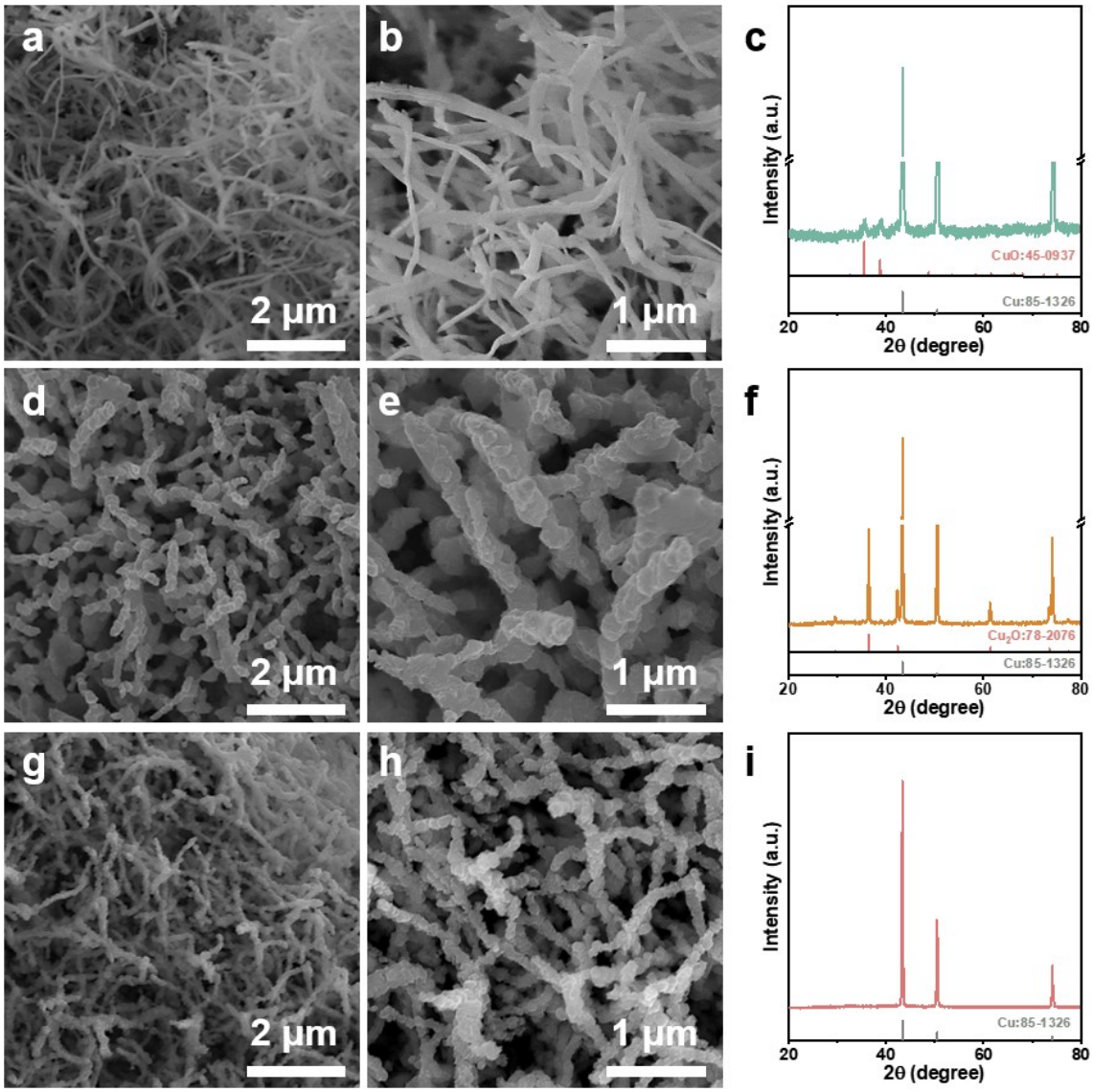

Fig. S2. (a, b, d, e, g, h) SEM images and (c, f, i) XRD patterns of (a-c) CuO/CF, (d-f) Cu_2O/CF, and (g-i) Cu/CF.

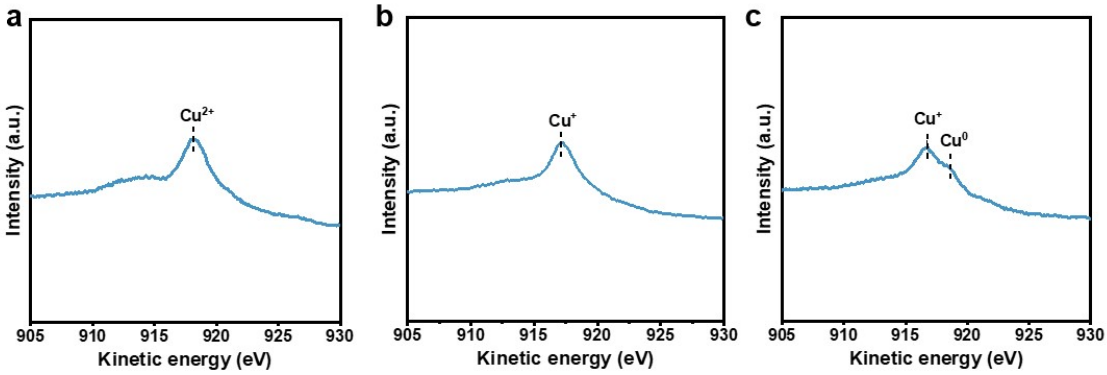

Fig. S3. Cu LMM Auger spectra of (a) CuO/CF, (b) Cu_2O/CF, and (c) Cu/CF.

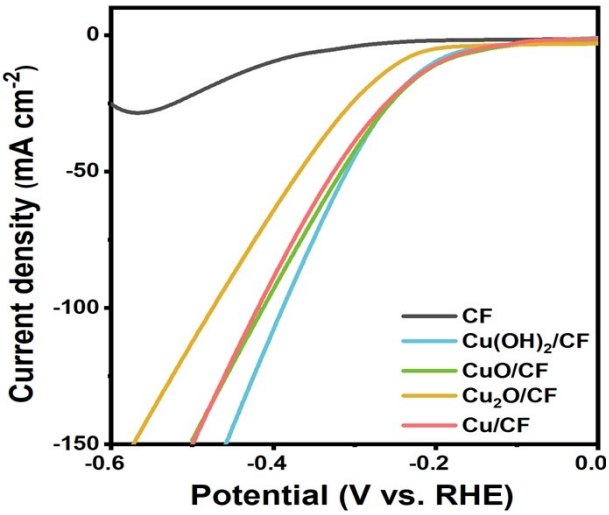

Fig. S4. LSV curves of various catalysts.

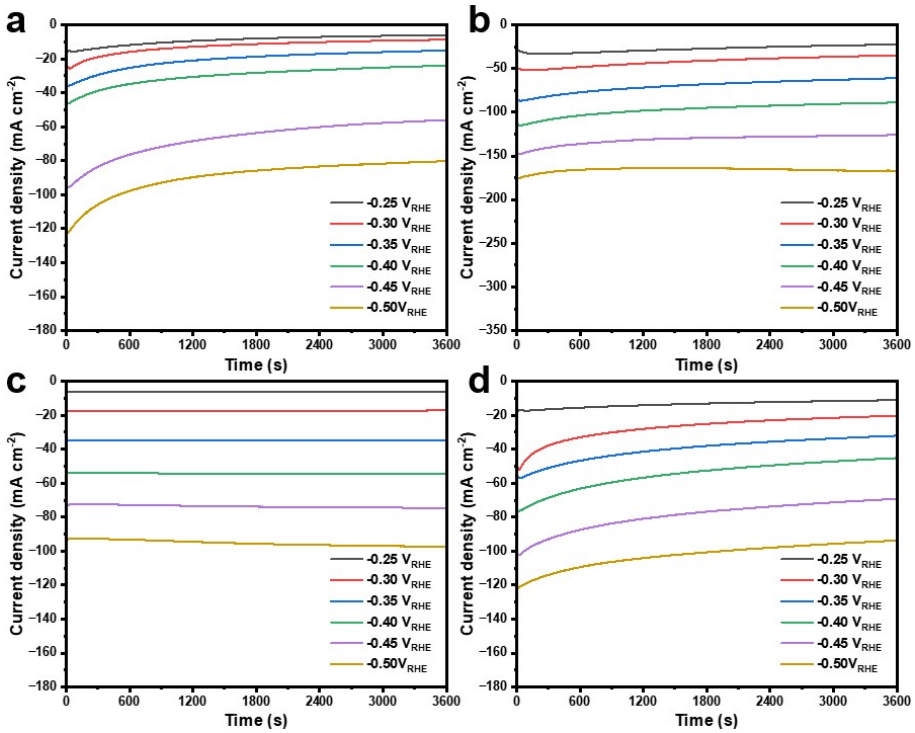

Fig. S5. i-t curves of different catalysts at potentials ranging from -0.25 V vs. RHE to -0.50 V vs. RHE: (a) $Cu(OH)_2$ NWs/CF; (b) CuO/CF , (c) Cu_2O/CF (d) Cu/CF.

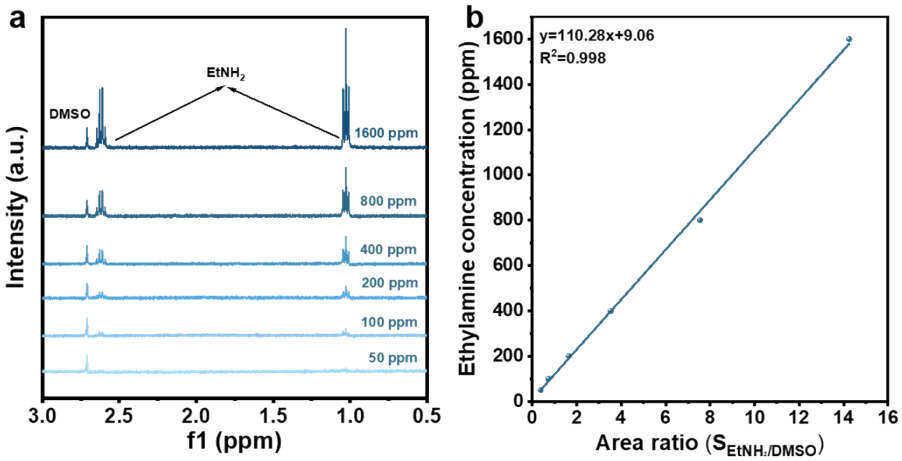

Fig. S6. (a) ^{1}H NMR spectra of ethylamine and (b) standard curve of ethylamine.

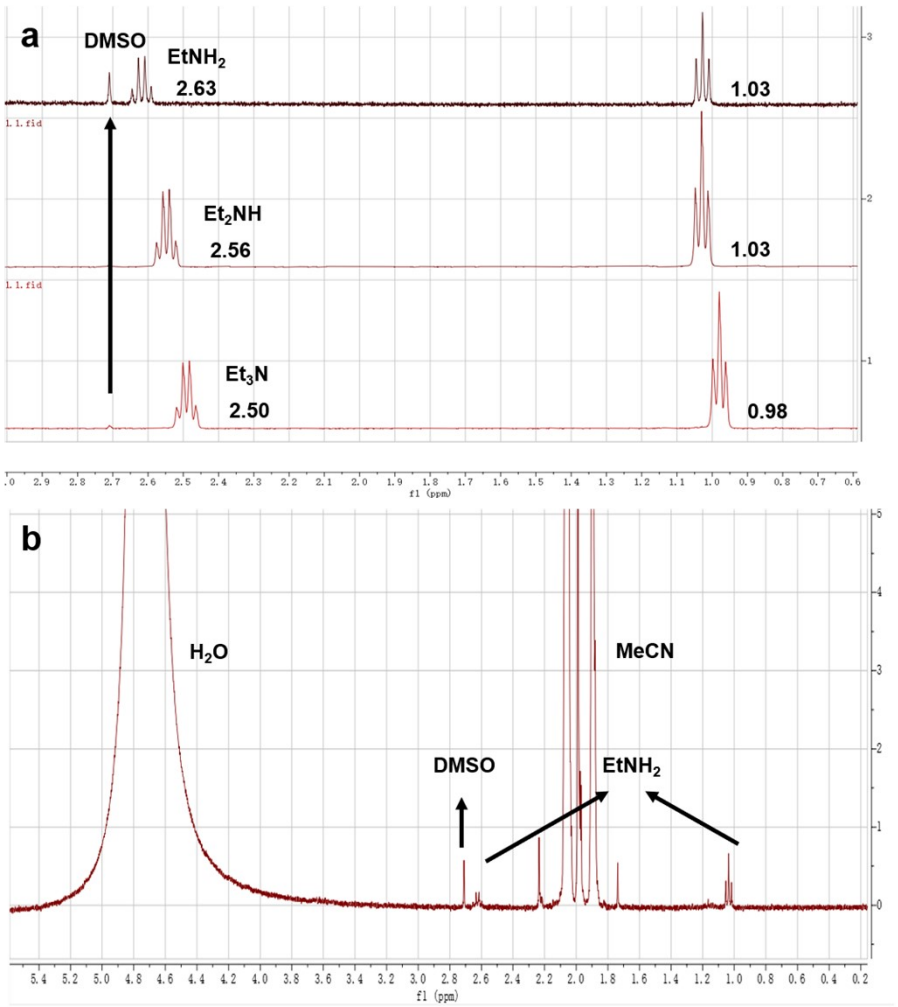

Fig. S7. (a) ^{1}H NMR spectra of standard solutions of ethylamine, diethylamine, and triethylamine; (b) ^{1}H NMR spectrum of the catholyte obtained after 1 h of electrolysis using $Cu(OH)_2$ NWs /CF at -0.35 V vs. RHE.

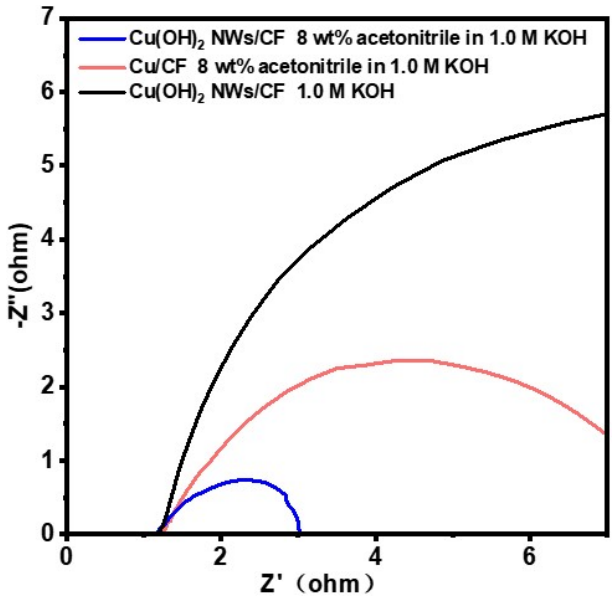

Fig. S9. Nyquist plots of $Cu(OH)_2$ NWs/CF and Cu/CF.

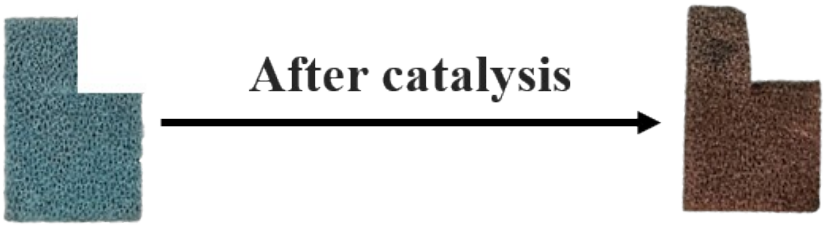

Fig. S10. Macroscopic morphology comparison of $Cu(OH)_2$ NWs/CF before and after ARR test.

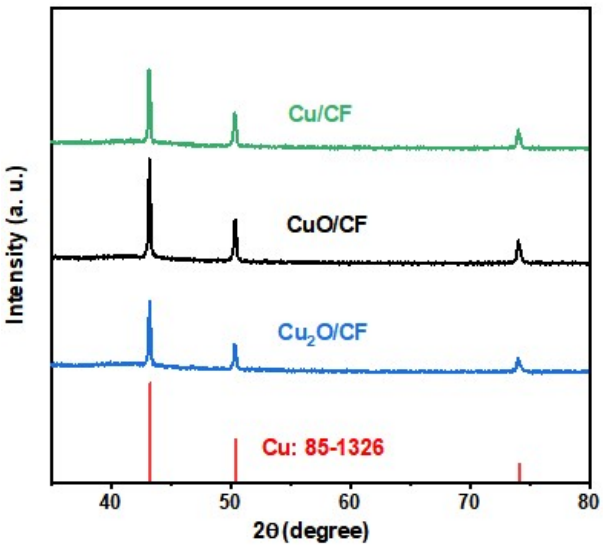

Fig. S11. XRD pattern of Cu/CF, CuO/CF, and Cu_2O/CF after ARR test.

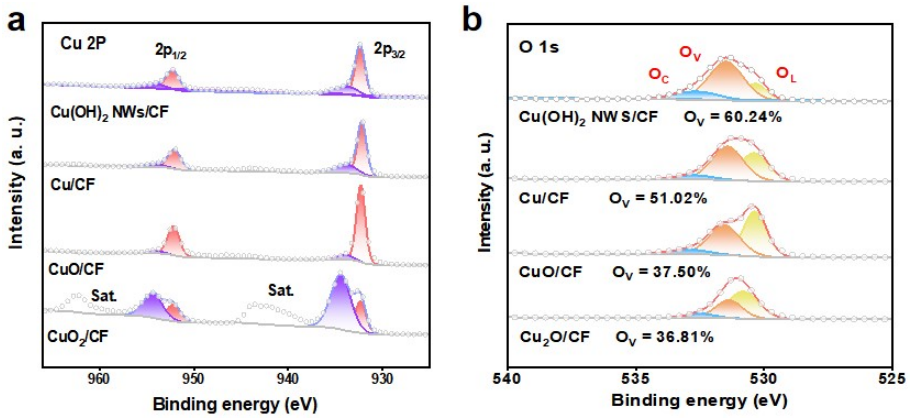

Fig. S12. (a) Cu 2p, (b) O 1s .XPS spectra of various electrocatalysts after ARR test.

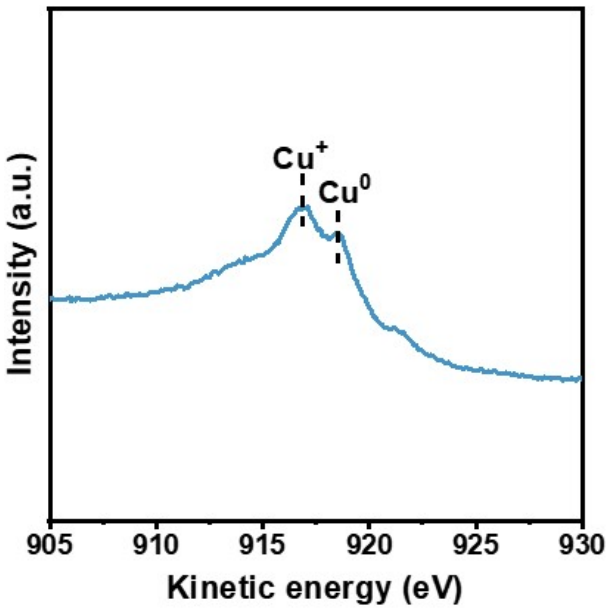

Fig. S13. LMM Auger spectra of $Cu(OH)_2$ NWs/CF after ARR test

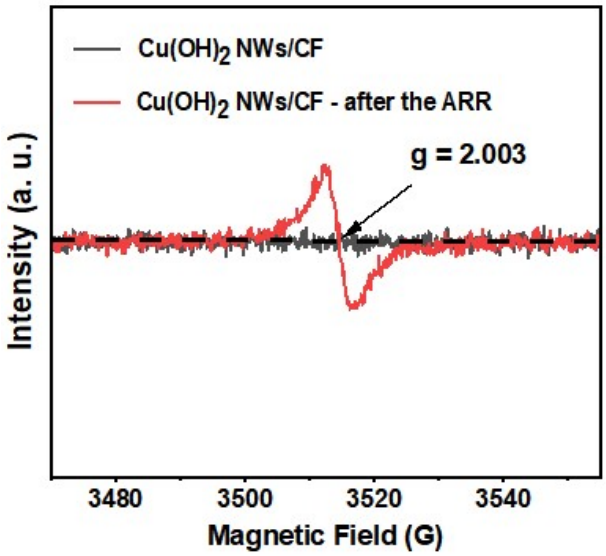

Fig. S14. EPR spectra of $Cu(OH)_2$ NWs/CF before and after ARR test.

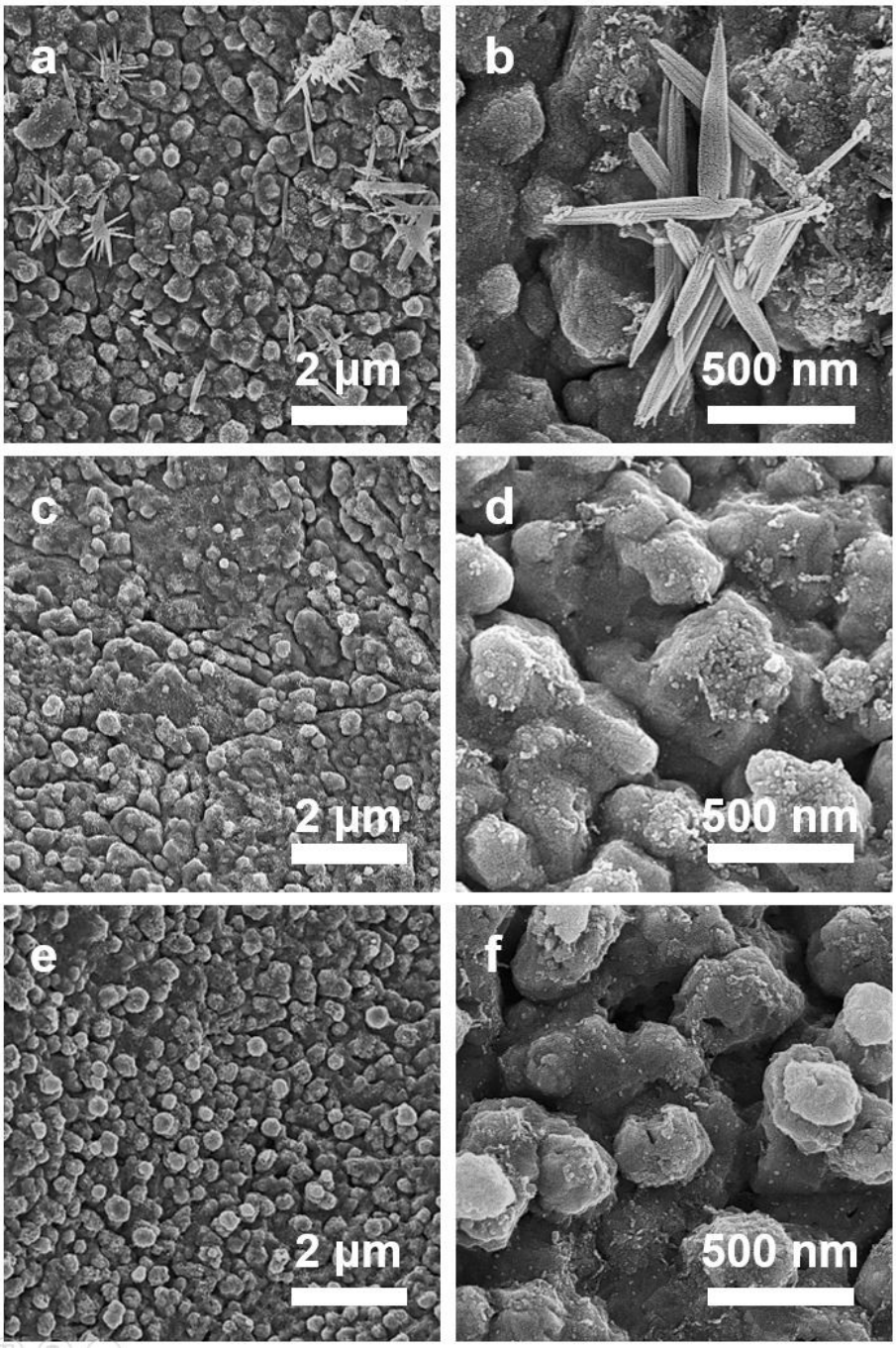

Fig. S15. SEM images of $Cu(OH)_2$ NWs/CF after ARR test: (a, b) 3 h; (c, d) 6 h; (e, f) 10 h.

Table S1. Performance comparison of various electrocatalysts for acetonitrile reduction to ethylamine.

Catalyst	Electrolyte	FE_{EA} (%)	yield rate	Stability	Ref.
$Cu(OH)_2$ NWs/CF	1 M KOH + 8 wt% CH_3CN	83.6	477.20 μmol h^{-1} cm^{-2}	Stable for 10 h, 10 h FE > 80%, H-type cell	**This work**
Rh ML	Ar-saturated 0.5M H_2SO_4 + 0.5M CH_3CN	56.7	137.1 μmol mg_{cat}^{-1} h^{-1}	Stable for 200 h, FE ＜ 56.7%, H-type cell	Carbon Energy, 2025, e70020
Cu@Ni–N–C	1 M NaOH + 8 wt% CH_3CN	> 98.65	793.8 μmol mg_{cat}^{-1} h^{-1}	Stable for 20 h, FE > 95%, H-type cell	Small, 2025, 2501419
Ni–N–C	1 M NaOH + 8 wt% CH_3CN	＜60	-	-	
Cu@C-1h	1 M KOH+12 wt% CH_3CN	98.2	2174 μmol mg_{cat}^{-1} h^{-1}	Stable for 12 h, FE > 83%, H-type cell test	Chem. Commun., 2025,61, 6494
Pd/C	0.5 M H_2SO_4+8 wt% CH_3CN	66.1	-	Stable for 45 h，FE > 35%, MEA	Nat Commun., 2024, 15, 3233
PdPtCuCoNi HEAAs	1 M NaOH + 8 wt% CH_3CN	83.51	677.13 mmol h^{-1} $g_{cat.}^{-1}$	-	Adv. Mater., 2024, 36, 2314142
PdPtCuCoNi HEAAs-400		90.75	746.82 μmol h^{-1} $mg_{cat.}^{-1}$	Stable for 50 h，10 circle FE ≈ 87.02%, H-type cell	
PdCu MAs/C	1 M NaOH + 8 wt% CH_3CN	69.3	-	Stable for 20 h，the current intensity in PdCu MAs/C gradually decreases by 45.90%	J. Energy Chem., 2024, 89, 216
PdCu MAs-400/C		88.6	316.0 μmol h^{-1} mg_{Pd+Cu}^{-1}	Stable for 20 h, excellent durability	
OD-Cu NWs	Ar-saturated 1 M KOH+8 wt% CH_3CN	82	-	Stability 16 h, FE ~ 80%, MEA	Nat Commun., 2023, 14, 3847
Cu NWs		93.4	-	-	
Pd-$Ni(OH)_2$ nanosheets	1 M KOH + 0.5 M CH_3CN	> 90	-	Stable for 8000 s, H-type cell	Angew. Chem. Int. Ed., 2023 e202307924
Cu_3Ni_1 MAs	1 M KOH + 8 wt% CH_3CN	95.49	173.2 μmol h^{-1}	Stable for 20 h, H-type cell	J. Mater. Chem. A, 2023, 11, 2210
Cu_3Ni_1 NPs		79.83	109.7 μmol h^{-1}	-	
Cu Nanoarrays (NAs)/Cu Foil	Ar-saturated 0.5 M $KHCO_3$ 0.5 M CH_3CN	~41	-	-	Chem. Catal., 2022, 2, 499
Cu Nanoarrays (NAs)/Cu Foil	CO_2-saturated 0.5 M $KHCO_3$ 0.5 M CH_3CN	~94	-	-	